PCCP

Accepted Manuscript

ROYAL SOCIETY OF CHEMISTRY

www.rsc.org/pccp

TOC

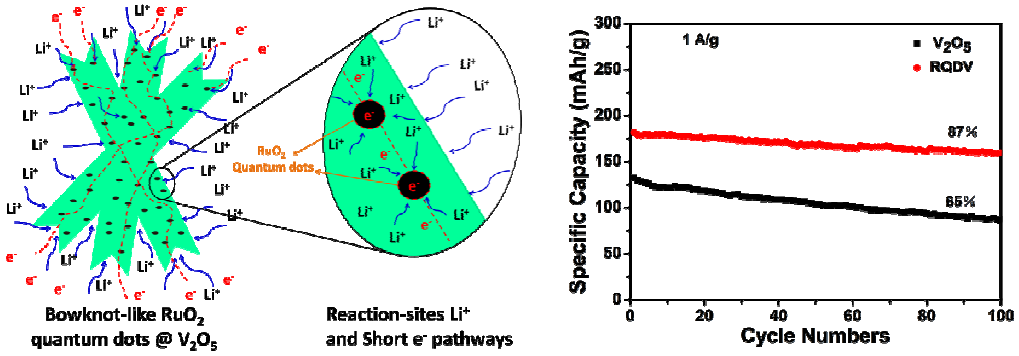

Text

Bowknot-like RuO_2 quantum dots @ V_2O_5 Cathode exhibits superior rate capability and cycling stability.

Physical Chemistry Chemical Physics RSCPublishing

COMMUNICATION

Bowknot-Like RuO_2 Quantum Dots @ V_2O_5 Cathode with Largely Improved Electrochemical Performance

Cite this: DOI: 10.1039/xoxxoooooox

Xiujuan Wei, Qinyou An, Qiulong Wei, Mengyu Yan, Xuanpeng Wang, Qidong Li Pengfei Zhang, Bolun Wang and Liqiang Mai*

Received ooth January 2012,
Accepted ooth January 2012

DOI: 10.1039/xoxxoooooox

www.rsc.org/

Bowknot-like RuO_2 quantum dots @ V_2O_5 nanomaterials have been synthesized by a facile hydrothermal method followed by annealing treatment, which exhibit largely enhanced electrochemical performance. Especially, RuO_2 quantum dots @ V_2O_5 cathode delivers 160 mAh/g at 1000 mA/g after 100 cycles, which is much higher than 86 mAh/g of the pure V_2O_5 cathode.

Introduction

With the global energy and environmental problems becoming more and more severe, the development of environment friendly and efficient energy storage systems are urgently required.[1,2] Lithium-ion batteries (LIBs) play an important role as energy storage devices for use in portable electronic devices, electric vehicles and electric grid due to their high energy-density, high safety and environmentally benign.[3-7] Among the potential cathode materials, vanadium pentoxide (V_2O_5) is the one of the most promising materials for LIBs owing to its low cost, high energy density, easy synthesis, as well as relatively high theoretical capacity of 294 mAh/g in the voltage range of 4.0–2.0 V vs. Li^+/Li.[8-10] Nevertheless, V_2O_5 suffers from low diffusion coefficient of Li^+, poor electrical conductivities (10^{-5}-10^{-3} S/cm) and poor structural stability, which limit the development of vanadium pentoxide electrode material in LIBs.[11-13]

In order to improve the electrochemical performances of V_2O_5 electrode materials, various nanostructure V_2O_5 have been successfully synthesized, including nanowires,[14,15] nanobelts,[16-18] nanotubes[19] and nanosheets.[20] These nanostructures can shorten the diffusion distance of Li^+ and accommodate large volume change during the lithium intercalation and de-intercalation processes.[21-23] Significant investigations have been carried out to develop unique nanostructured materials.[24, 25] For example, Shi et al. synthesized the LiV_3O_8 thin film with a mixed amorphous-nanocrystalline exhibiting high capacity and good capacity retention.[26] Besides, the transportation of electrons within the electrode also exerts a significant impact on the rate capability of LIBs. The resistance is arising from the low electronic conductivity of the electrode materials. Thus, it is required to use V_2O_5 in conjunction with another nanostructured material possessing higher electronic conductivity.[27-30] For example, Chen et al. constructed the MWCNT/V_2O_5 core/shell sponge for high power density.[31] Zhang et al. fabricated carbon-coated V_2O_5 with high performance.[32] RuO_2 exhibits high electronic conductivity (2.5×10^4 S/cm), fast Li^+ permeation and stable reaction interface (high coulombic efficiency above 98%), which has been extensively studied by many researchers.[33-35] Maier and co-workers reported that using RuO_2 improved electrode performance of Porous $LiFePO_4$.[33] RuO_2-containing composites reveal reversible capacities of 124 and 93 mAh/g at rates of 2 C and 10 C, respectively. It is worth noting that quantum dots (QDs) with small size shorten the diffusion length for Li^+, which is beneficial to achieve cycling stability and rate capability. Han et al. constructed the V_2O_5 QDs/graphene hybrid nanocomposite exhibiting stable cycling ability and high reversible capacity.[36] Mo et al. also synthesized the TiO_2 QDs/graphene nanosheets, which revealed enhanced electrochemical performance.[37]

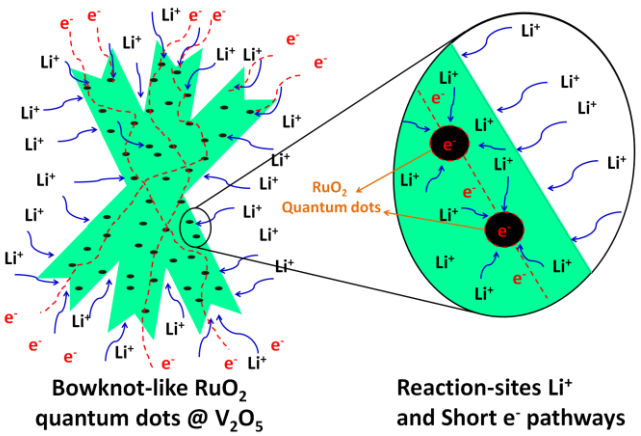

Scheme 1. Schematic illustration of the bowknot-like RuO_2 quantum dots @ V_2O_5 with accessible intercalation sites for Li^+ and short electron/ion transport pathways.

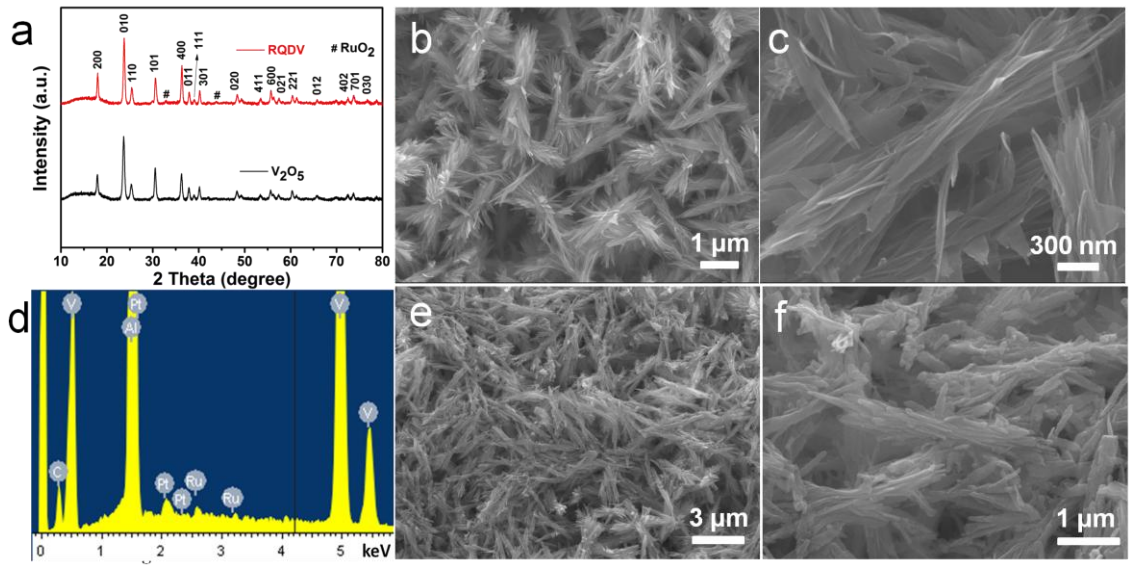

Figure 1 (a) The XRD patterns of the prepared V_2O_5 and RQDV; (b-c) the low and high magnification FESEM images of RQDV precursor, respectively; (d) The EDX pattern of RQDV; (e-f) the low and high magnification FESEM images of RQDV, respectively.

Here in, to take the advantages of RuO_2, QDs and V_2O_5, we designed and synthesized bowknot-like RuO_2 quantum dots @ V_2O_5 (denoted as RQDV) nanomaterials via a facile and rapid hydrothermal synthesis method followed by annealing treatment. To our knowledge, the bowknot-like RQDV was not reported before. As shown in **Scheme 1**, the RuO_2 QDs have excellent electronic conductivity and fast Li^+ permeation.[34] The RuO_2 QDs disperse on the bowknot-like V_2O_5 that enhance the electronic conductivity of this material. The unique nanostructure with RuO_2 QDs dispersing on the V_2O_5 offers multi-intercalation sites for Li^+ and short electron transport pathways. The RQDV cathode shows higher rate capability and better cycling stability than the pure V_2O_5 cathode.

Experimental section

Sample preparation

The RQDV was synthesized as follows: vanadium pentoxide (V_2O_5) powder (1mmol) dispersed in deionized water (30mL) and hydrogen peroxide solution (5 mL, 30%) was added under stirring until clear orange solution formed. After that, ammonium dihydrogen phosphate ($NH_4H_2PO_4$) (1.5 mmol) was added in the solution. Then, 0.08 mmol Ruthenium chloride solution was added to above solution. Finally, the resulting solution was transferred into a telfon-lined stainless steel autoclave and kept at 180 ^oC for 3 h. The products were washed repeatedly with deionized water and ethanol, and finally dried at 70 ^oC for 12 h. The as-prepared samples were annealed at 450 ^oC for 3 h at a ramping rate of 3 ^oC /min.

The sample after the hydrothermal process followed by annealing prepared with 0.08 mmol $RuCl_3$ is marked as RQDV. The sample without $RuCl_3$ after annealing is marked as the pure V_2O_5. The sample without annealing is marked RQDV precursor.

Material characterization

X-ray diffraction (XRD) measurements were performed to obtain the crystallographic information using a D8 Advance X-ray diffractometer with a non-monochromated Cu Ka X-ray source. Field emission scanning electron microscopic (FESEM) images and energy dispersive spectra (EDS) were collected using a JEOL-7100F microscopy. X-ray photoelectron spectroscopy (XPS) analysis was done on VG Multilab 2000. Transmission electron microscopic (TEM) and high-resolution TEM (HRTEM) images were recorded using a JEOL JEM-2100F STEM/EDS microscope. X-Ray Fluorescence (XRF) analysis was conducted on Axios advanced X-ray fluorescence spectrometer JY/T 016-1996.

Electrochemical measurements

The electrochemical measurements were carried out by assembly of 2016 coin cells in a glove box filled with pure argon gas, using lithium discs as both the counter electrode and the reference electrode, and 1 M $LiPF_6$ in a mixture of ethylene carbon/dimethyl carbonate (1 : 1 w/w) as electrolyte. Cathodes were obtained with 70% active material, 20% acetylene black and 10% poly (tetrafluoroethylene) (PTFE). Galvanostatic charge-discharge tests were performed at a potential range of 2.0-4.0 V vs. Li^+/Li using a multichannel battery testing system (LAND CT2001A). Cyclic voltammetry (CV) and electrochemical impedance spectra (EIS) were tested with an electrochemical workstation (Autolab PGSTAT 302N).

Results and discussion

Figure 1a shows the XRD patterns of the pure V_2O_5 and RQDV. The pure V_2O_5 matches well with orthorhombic V_2O_5 phase (JCPDS card No. 00-001-0359) with no impurity phase. The as-prepared RQDV is well crystallized and exhibits the standard diffraction peaks of orthorhombic V_2O_5 phase. In addition, the standard diffraction peaks of RuO_2 also exists corresponding to JCPDS card No. 00-050-1428, which reveals that RuO_2 forms during the synthesis process. The forming mechanism of the RuO_2 QDs may be due to the hydrogen peroxide in the solution converting Ru (III) to RuO_2 nanoparticles in hydrothermal process at 180 ^oC and subsequent crystallization in the annealing process.[38, 39] The XRD pattern of RQDV precursor (ESI†, Figure S1) was also measured. The peak intensity of RQDV precursor is very weak, which indicates RQDV precursor has very low crystallinity. Figure 1b shows the low magnification FESEM image of the RQDV precursor, which

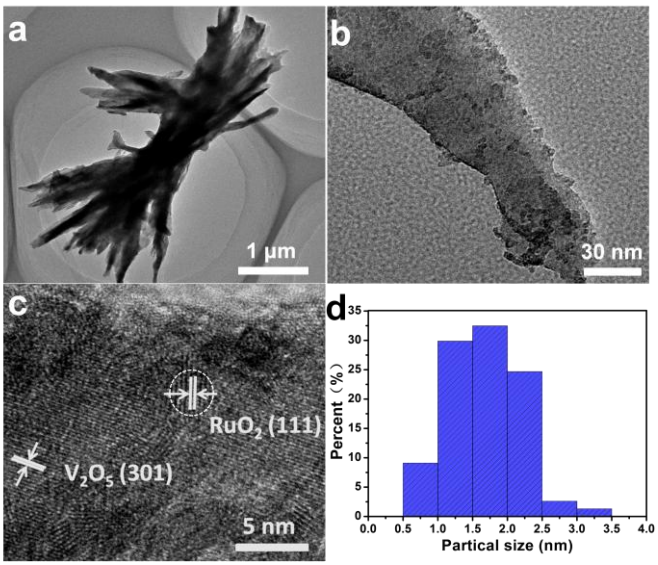

Figure 2 (a) The low, (b) the high magnification TEM images and (c) the high-resolution TEM (HRTEM) images of the annealed RQDV, respectively. (d) Particle size distribution of RuO_2 QDs on V_2O_5.

presents uniform bowknot-liked structures. The high magnification FESEM image (Figure 1c) shows that bowknot-liked structures are composed of hierarchical assemblies of single nanosheet with transverse diameter of 50~200 nm. The EDS analysis of the bowknot-liked nanomaterials indicates their chemical composition corresponding well to that of the RQDV (Figure 1d). Figure 1e and 1f represent the low and high magnification FESEM image of the RQDV, respectively. It can be seen that the bowknot-liked structures can retain well after calcinations. The low magnification FESEM image of the pure V_2O_5 precursors presents that nanobelts extend continuously around a center (ESI†, Figure S2a) The morphology of this sample can be further observed by the high magnification FESEM image, which shows the structure of nanoribbons with an average diameter of ~100 nm (ESI†, Figure S2b). After annealing, some nanobelts were damaged and aggregated (ESI†, Figure S2c and 2d).

Time-dependent experiments were conducted to further understand the formation process of such bowknot-like structures. The samples were collected at different stages of the synthesis process, and their morphologies were investigated by SEM (ESI†, Figure S3). When the reaction time is just 30 min, the some nanosheets were formed and aggregated (ESI†, Figure S3a). As the reaction time increased to 1h, more nanosheets formed and constructed into bowknot-like structures (ESI†, Figure S3b). With the reaction prolonging to 2 h, some nanoflowers assembled by nanosheets through the Ostwald ripening process can be observed (ESI†, Figure S3c). As the reaction time increased to 6h, bowknot-like structures were formed, which were similar to the initial stage (ESI†, Figure S3d).

Figure 2a shows the low magnification TEM image of the annealed RQDV, which further indicates the high thermal stability of the bowknot-liked structure. The high magnification TEM image of annealed RQDV (Figure 2b) exhibits nanometer-sized RuO_2 (0.5-3.5 nm) dispersed on the surface of V_2O_5. Figure 2c shows the high resolution transmission electron microscopy (HRTEM) of the annealed RQDV. The lattice spacing of 2.61 Å is indexed to the (301) set of planes of the orthorhombic V_2O_5 (JCPDS card No. 00-001-0359), it can be also observed that the lattice spacing of 2.79 Å indexed to the (111) set of planes of the RuO_2 (JCPDS card No. 00-050-1428) exists. The particle size distribution of RuO_2 is obtained through statistically analyzing the HRTEM of the RQDV (Figure 2d). It exhibits that over 80% of the QDs are in the size range of 1-2.5 nm.

XRF analysis was performed to examine the composition of annealed RQDV. The XRF table shows that the as-obtained samples mainly contain V_2O_5 and RuO_2, which reveals that the mass percentage of RuO_2 is 2.56% in the composite (ESI†, Table S1). XPS measurements were conducted to further confirm the oxidation state of vanadium and ruthenium. Figure 3a shows the binding energy for V $2p_{3/2}$ at 517.2 eV, which corresponds to V^{5+} in V_2O_5 according with the previous report.[40] Figure 3b represents the spectra for $Ru3d_{5/2}$ and C1s. The $Ru3d_{5/2}$ band was observed at 281.0 eV attributing to Ru^{4+} in RuO_2.[41] C1s band at 284.6 eV may be from the effect of the atmosphere.[42]

Various electrochemical measurements were performed to contrast the electrochemical performances of the as-prepared samples (Figure 4). The cyclic voltammetry (CV) curve of the RQDV electrode was test at a scan rate of 0.1 mV/s in the potential range from 2.0 to 4.0 V (Figure 4a). It is clear that three pairs of redox peaks appear at 2.588/2.196, 3.291/3.118 and 3.493/3.323 V, which can be attributed to the Li-ion insertion and extraction processes, corresponding to the phase transitions from α-V_2O_5 to ε-$Li_{0.5}V_2O_5$, ε- $Li_{0.5}V_2O_5$ to δ- LiV_2O_5 and δ- LiV_2O_5 to γ- $Li_2V_2O_5$, respectively (Equation 1-3).[43]

$$V_2O_5 + 0.5Li^+ + 0.5e^- = \varepsilon\text{-}\ Li_{0.5}V_2O_5 \quad (1)$$

$$\varepsilon\text{-}\ Li_{0.5}V_2O_5 + 0.5Li^+ + 0.5e^- = \delta\text{-}\ LiV_2O_5 \quad (2)$$

$$\delta\text{-}\ LiV_2O_5 + Li^+ + e^- = \gamma\text{-}\ Li_2V_2O_5 \quad (3)$$

The cyclic voltammetry curve of the pure V_2O_5 was also tested at a scan rate of 0.1 mV/s in the potential range from 2.0 to 4.0 V (ESI†, Figure S4a). The three main cathodic and anodic peaks correspond to a series of phase transformation. The shape of the pure V_2O_5 is similar to that of the RQDV. However, there are some minor peaks, which may result from structural changes. Figure 4b shows the charge-discharge voltage profiles

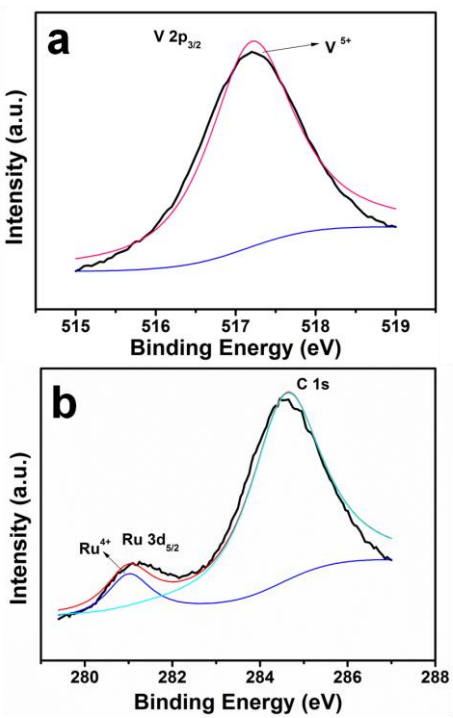

Figure 3 The XPS spectra for annealed RQDV: (a) the V $2p_{3/2}$ bands; (b) the Ru $3d_{5/2}$ and C1s bands.

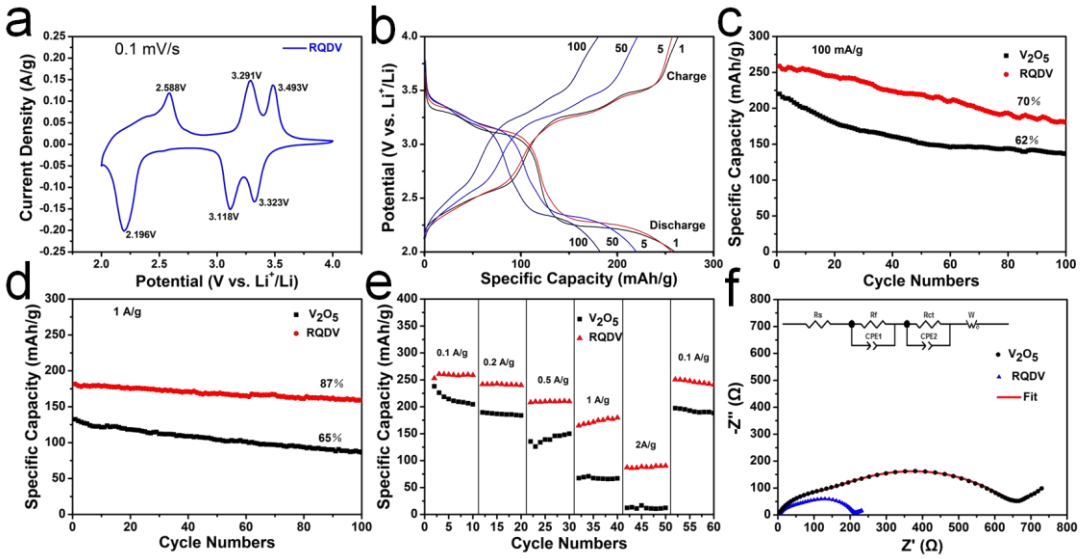

Figure 4 (a) Representative CV curve of an electrode based on the RQDV electrode obtained at a voltage range of 2.0 to 4.0 V (vs Li^+/Li) at scan rate of 0.1 mV/s; (b) Voltage profiles plotted for the first, fifth, 50th and 100th cycles of RQDV composite electrode at a current density of 100 mA/g; (c, d) The cycling performances of the pure V_2O_5 and RQDV electrodes at the current densities of 100 mA/g and 1 A/g, respectively; (e) the rate performances of the pure V_2O_5 and RQDV electrodes at different current densities; (f) The Nyquist plots of the pure V_2O_5 and RQDV electrodes.

for the 1st, 5th, 50th and 100th cycles of RQDV electrode at a current density of 100 mA/g. There are three voltage plateaus observed in the discharge process, which are accorded with the redox peaks in CV curves. The charge-discharge voltage profiles for the 1st, 5th, 50th and 100th cycles of the pure V_2O_5 electrode were collected at a current density of 100 mA g^{-1} (ESI†, Figure S4b). When the cycling numbers reach to 50th and 100th cycles, the pure V_2O_5 shows poor reversibility.

Figure 4c and 4d show the cycling performances of the pure V_2O_5 and RQDV tested via constant current charge-discharge in a voltage range of 2.0-4.0V cycling up to 100 cycles, which demonstrate the superiority of the RQDV as cathode material. Figure 4c shows the cycling ability comparison of the pure V_2O_5 and RQDV at the current density of 100 mA/g. The capacity retentions of the pure V_2O_5 and RQDV after 100 cycles are 62% and 70%, respectively. RQDV reveal the better cycling performance delivering relatively high capacity, which may be ascribed to its unique nanostructures with RuO_2 QDs dispersing on the V_2O_5. The cycling performances of the pure V_2O_5 and RQDV electrodes also were tested at a current density of 1 A/g (Figure 4d). Comparing with RQDV, the pure V_2O_5 delivered a lower capacity of 86 mAh/g after 100 cycles. The capacity retention of the pure V_2O_5 only remains 65% after 100 cycles, while the capacity retention of RQDV still remains 87%. The RQDV clearly exhibits the excellent cycling performance. The capacity retention at 1 A/g after 100 cycles was much higher than that at 100 mA/g. Such electrochemical performances may be caused by the following reasons: there are more Li^+ intercalation/de-intercalation in the internal structure of RQDV electrode at the low current of 100 mA/g, the structure of material may be more serious damaged than that at the high current of 1 A/g during the charge and discharge process. Similar phenomena are also reported.[44] The rate performances of the pure V_2O_5 and RQDV were studied at different charge/discharge rates from 100 to 2000 mA/g (Figure 4e). The RQDV electrode shows 175 and 90 mAh/g, which is much higher than that of the pure V_2O_5 electrode (88 and 11 mAh/g) at the current densities of 1000 and 2000 mA/g, respectively. The RQDV exhibits much better electrochemical performance compared with the pure V_2O_5, especially at the high current density, which further demonstrates the advantage of the RQDV as LIBs cathode materials. Figure 4f shows the electrochemical impedance spectra of the pure V_2O_5 and RQDV electrodes. The Nyquist plots show that the charge transfer resistance (R_{ct}) of RQDV (139 Ω) is much smaller than that of the pure V_2O_5 (549 Ω), which indicate that the charge transfer kinetics of RQDV is faster than that of the pure V_2O_5.[45, 46]

The RQDV cathode exhibits higher rate performance and better cyclic stability in comparison with the pure V_2O_5 cathode. The RQDV cathode still delivers 160 mAh/g at the high current density of 1000 mA/g after 100 cycles, which is much higher than 86 mAh/g of the pure V_2O_5 cathode. Especially, it still delivers capacity of 90 mAh/g at the high current density of 2000 mA/g, whereas the capacity of the pure V_2O_5 is negligible. The electrochemical performances of RuO_2 QDs @ V_2O_5 are also carefully compared with other previous works (Table S2). The RQDV shows good cyclic stability and superior rate performance. The impressive electrochemical performances of RQDV can be attributed to the following advantages: 1) the unique RQDV nanostructure offers accessible intercalation sites and shortens Li^+ and electronic transport pathways, which favors electrolyte penetration and interface reactions;[36, 47, 48] 2) RuO_2 QDs are dispersed on the electrode surface, which enhances the electronic conductivity of this material. The effect of introducing RuO_2 QDs is remarkable. This point has also been confirmed by other reports.[33, 49]

Conclusions

In summary, we have successfully synthesized the RuO_2 quantum dots @ bowknot-like V_2O_5 nanomaterials by a facile hydrothermal synthesis method followed by annealing treatment at 450 °C in air. The RuO_2 QDs have the diameter of 0.5-3.5 nm. The electrochemical tests demonstrate that the RQDV cathode exhibits the enhanced electrochemical performance. Especially, it delivers capacity of 160 mAh/g at

the high current density of 1000 mA/g and improves cycling stability (87% capacity retention after 100 cycles), whereas the capacity for the pure V_2O_5 is 86mAh/g (65% capacity retention after 100 cycles). The enhanced electrochemical performance can be ascribed to the unique nanostructure with RuO_2 QDs dispersing on the electrode surface. This strategy can be also an effective technique for improving the electrochemical performance of other electrodes especially at high rate.

Acknowledgements

This work was supported by the National Basic Research Program of China (2013CB934103, 2013DFA50840), the National Natural Science Foundation of China (51272197) and the Fundamental Research Funds for the Central Universities (2013-VII-028, 2014-YB-001, 2014-YB-002).

Notes and references

[a] State Key Laboratory of Advanced Technology for Materials Synthesis and Processing, WUT-Harvard Joint Nano Key Laboratory, Wuhan University of Technology, Wuhan, 430070, P. R. China. E-mail: mlq518@whut.edu.cn; Fax: +86-027-87644867; Tel: +86-027-87467595

All authors discussed the results and commented on the manuscript. The authors declare no competing financial interest.

† Electronic Supplementary Information (ESI) available: [The XRD patterns of the prepared RQDV precursor; the low and high magnification FESEM images of the RQDV precursor, respectively; FESEM images of the RQDV precursor obtained at different hydrothermal time: 30 min, 1 h, 2 h and 6 h; representative CV curve of an electrode based on the V_2O_5 electrode obtained at a voltage range of 2.0 to 4.0 V (vs Li^+/Li) at scan rate of 0.1 mV/s; voltage profiles plotted for the 1^{st}, 5^{th}, 50^{th} and 100^{th} cycles of V_2O_5 electrode at a current density of 100 mA/g; XRF of the RQDV]. See DOI: 10.1039/c000000x/

1 P. Yang and J.M. Tarascon, *Nat. Mater.* , 2012, **11**, 560.
2 B. Kang and G. Ceder, *Nature*, 2009, **458**, 190.
3 M. Armand and J.-M. Tarascon, *Nature*, 2008, **451**, 652.
4 L. Hu, H. Wu, F. L. Mantia, Y. Yang and Y. Cui, *ACS Nano*, 2010, **4**, 5843.
5 N. Mahmood, C. Zhang, H. Yin and Y. Hou, *J. Mater. Chem. A*, 2014, **2**, 15.
6 R. Hu, W. Sun, H. Liu, M. Zeng and M. Zhu, *Nanoscale*, 2013, **5**, 11971.
7 Y. Yao, M. T. McDowell, Ill Ryu, H. Wu, N. Liu, L. Hu, W. D. Nix and Y. Cui, *Nano Lett.*,2011, 11, 2949.
8 S. Wang, S. Li, Y. Sun, X. Feng and C. Chen, *Energy Environ. Sci.*, 2011, **4**, 2854.
9 M. S. Whittingham, *Chem. Rev.*, 2004, **104**, 4271.
10 V. Raju, J. Rains, C. Gates, W. Luo, X. Wang, W. F. Stickle, G. D. Stucky and X. Ji, *Nano Lett.*, 2014, DOI: 10.1021/nl501692p.
11 H. Yu, X. Rui, H. Tan, J. Chen, X. Huang, C. Xu, W. Liu, Y. Denis, H. H. Hng and H. E. Hoster, *Nanoscale*, 2013, **5**, 4937.
12 R. Baddour-Hadjean, J. Pereira-Ramos, C. Navone and M. Smirnov, *Chem. Mater.*, 2008, **20**, 1916.
13 L. Mai, F. Dong, X. Xu, Y. Luo, Q. An, Y. Zhao, J. Pan and J. Yang, *Nano Lett.*, 2013, **13**, 740.
14 L. Mai, L. Xu, C. Han, X. Xu, Y. Luo, S. Zhao and Y. Zhao, *Nano Lett.*, 2010, **10**, 4750.
15 J. W. Lee, S. Y. Lim, H. M. Jeong, T. H. Hwang, J. K. Kang and J. W. Choi, *Energy Environ. Sci.*, 2012, **5**, 9889.
16 J. Liu, X. Wang, Q. Peng and Y. Li, *Adv. Mater.*, 2005, **17**, 764.
17 B. Li, Y. Xu, G. Rong, M. Jing and Y. Xie, *Nanotechnology*, 2006, **17**, 2560.
18 Y. Wang, H. J. Zhang, W. X. Lim, J. Y. Lin and C. C. Wong, *J. Mater. Chem.*, 2011, **21**, 2362.
19 V. Mohan, B. Hu, W. Qiu and W. Chen, *J. Appl. Electrochem.*, 2009, **39**, 2001.
20 Q. An, Q. Wei, L. Mai, J. Fei, X. Xu, Y. Zhao, M. Yan, P. Zhang and S. Huang, *Phys. Chem. Chem. Phys.*, 2013, **15**, 16828.
21 Y. Wang and G. Cao, *Adv. Mater.*, 2008, 20, 2251.
22 A. M. Cao, J. S. Hu, H. P. Liang and L. J. Wan, *Angew. Chem. Int. Ed.*, 2005, **44**, 4391.
23 D. Yu, C. Chen, S. Xie, Y. Liu, K. Park, X. Zhou, Q. Zhang, J. Li and G. Cao, *Energy Environ. Sci.*, 2011, **4**, 858.
24 Q. Shi, J. Liu, R. Hu, M. Zeng, M. Dai and M. Zhu, *RSC Advances*, 2012, **2**, 7273.
25 M. G. Kim and J. Cho, *Adv. Funct. Mater.*, 2009, **19**, 1497.
26 Q. Shi, R. Hu, L. Ouyang, M. Zeng and M. Zhu, *Electrochem. Commun.*, 2009, **11**, 2169.
27 Y. Wei, C.W. Ryu and K.B. Kim, *J. Power Sources*, 2007, **165**, 386.
28 F. S. Gittleson, J. Hwang, R. C. Sekol and A. D. Taylor, *J. Mater. Chem A*, 2013, **1**, 7979.
29 Z. Li and E. Ruckenstein, *Langmuir*, 2002, **18**, 6956.
30 L. Xu, Y. Liu, M. P. Garrett, B. Chen and B. Hu, *J. Phys. Chem. C*, 2013, **117**, 10264.
31 X. Chen, H. Zhu, Y.-C. Chen, Y. Shang, A. Cao, L. Hu and G. W. Rubloff, *ACS Nano*, 2012, **6**, 7948.
32 X. F. Zhang, K. X. Wang, X. Wei and J.-S. Chen, *Chem. Mater.*, 2011, **23**, 5290.
33 Y. S. Hu, Y. G. Guo, R. Dominko, M. Gaberscek, J. Jamnik and J. Maier, *Adv. Mater.*, 2007, **19**, 1963.
34 P. Balaya, H. Li, L. Kienle and J. Maier, *Adv. Funct. Mater.*, 2003, **13**, 621.
35 E. Bekaert, P. Balaya, S. Murugavel, J. Maier and M. Ménétrier, *Chem. Mater.*, 2009, **21**, 856.
36 C. Han, M. Yan, L. Mai, X. Tian, L. Xu, X. Xu, Q. An, Y. Zhao, X. Ma and J. Xie, *Nano Energy*, 2013, **2**, 916.
37 R. Mo, Z. Lei, K. Sun and D. Rooney, *Adv. Mater.*, 2014, **26**, 2084.
38 H. Wang, Y. Liang, T. Mirfakhrai, Z. Chen, H. S. Casalongue and H. Dai, *Nano Res.*, 2011, **4**, 729.
39 H. Yu, K. Zeng, X. Fu, Y. Zhang, F. Peng, H. Wang and J. Yang, *J. Phys. Chem. C*, 2008, **112**, 11875.
40 M. Sathiya, A. Prakash, K. Ramesha, J. M. Tarascon and A. Shukla, *J. Am. Chem. Soc.*, 2011, **133**, 16291.
41 C. S. Huang, M. Houalla, D. M. Hercules, C. L. Kibby and L. Petrakis, *J. Phys. Chem.*, 1989, **93**, 4540.
42 C. Yang, G. Wang, Z. Lu, J. Sun, J. Zhuang and W. Yang, *J. Mater. Chem.*, 2005, **15**, 4252.
43 A. Pan, J.G. Zhang, Z. Nie, G. Cao, B. W. Arey, G. Li, S.Q. Liang and J. Liu, *J. Mater. Chem.*, 2010, **20**, 9193.
44 R. Yu, C. Zhang, Q. Meng, Z. Chen, H. Liu and Z. Guo, *Appl. Mater. Interfaces*, 2013, **5**, 12394.

45 Q. Wei, Q. An, D. Chen, L. Mai, S. Chen, Y. Zhao, M. H. Kalele, L. Xu, A. M. Khan and Q. Zhang, *Nano Lett.*, 2014, **14**, 1042.
46 L. Shen, H. Li, E. Uchaker, X. Zhang and G. Cao, *Nano Lett.*, 2012, **12** , 5673.
47 J. G. Kang, J. G. Park and D. W. Kim, *Electrochem. Commun.*, 2010, **12**, 307.
48 F. Croce, A. D Epifanio, P. Reale, L. Settimi and B. Scrosati, *J. Electrochem. Soc.*, 2003, **150**, A576.
49 F. Zhang, S. Passerini, B. B. Owens and W. H. Smyrl, *Electrochem. Solid-State Lett.*, 2001, **4**, A221.

